Journal of Biomolecular NMR, **22:** 153–164, 2002.
KLUWER/ESCOM

Sequence-specific assignment of histidine and tryptophan ring ^{1}H, ^{13}C and ^{15}N resonances in ^{13}C/^{15}N- and ^{2}H/^{13}C/^{15}N-labelled proteins

Frank Löhr*, Vicky Katsemi, Marco Betz, Judith Hartleib & Heinz Rüterjans
Institut für Biophysikalische Chemie, Johann Wolfgang Goethe-Universität Frankfurt am Main, Biozentrum N230, 1. OG, Marie Curie-Strasse 9, D-60439 Frankfurt, Germany

Received 1 October 2001; Accepted 12 November 2001

Key words: aromatic resonance assignment, DFPase, perdeuteration, triple-resonance NMR, TROSY, xylanase

Abstract

Methods are described to correlate aromatic $^{1}H^{\delta 2}/^{13}C^{\delta 2}$ or $^{1}H^{\varepsilon 1}/^{15}N^{\varepsilon 1}$ with aliphatic $^{13}C^{\beta}$ chemical shifts of histidine and tryptophan residues, respectively. The pulse sequences exclusively rely on magnetization transfers via one-bond scalar couplings and employ [^{15}N, ^{1}H]- and/or [^{13}C, ^{1}H]-TROSY schemes to enhance sensitivity. In the case of histidine imidazole rings exhibiting slow HN-exchange with the solvent, connectivities of these proton resonances with β-carbons can be established as well. In addition, their correlations to ring carbons can be detected in a simple [^{15}N, ^{1}H]-TROSY-H(N)C^{ar} experiment, revealing the tautomeric state of the neutral ring system. The novel methods are demonstrated with the 23-kDa protein xylanase and the 35-kDa protein diisopropylfluorophosphatase, providing nearly complete sequence-specific resonance assignments of their histidine δ-CH and tryptophan ε-NH groups.

Introduction

Aromatic amino acid residues are frequently located in the hydrophobic interior of proteins. As a consequence, they are involved in a large number of long-range NOE contacts relevant for solution structure determinations. Histidines, in particular, often occur at the active site of enzymes. The chemical shifts of histidine imidazole rings are important reporters of its protonation state, tautomeric structure, solvent accessibility and hydrogen-bonding status and can therefore contribute to the understanding of functional properties, be it enzyme activity or protein-ligand interactions. On the other hand, the determination of global folds of larger, perdeuterated proteins is hampered by their low proton densities and the concomitant limited number of available NOEs, implying that the knowledge of chemical shifts of exchangeable side-chain nuclei, such as $HN^{\varepsilon 1}$ in tryptophanes and possibly $HN^{\delta 1}$ or $HN^{\varepsilon 2}$ in histidines, is of particular importance for that purpose (Venters et al., 1995).

The crucial step in the sequence-specific assignment of aromatic resonances is the intraresidual link across the quarternary γ-carbon. The traditional assignment strategy is based on through-space interactions between α- and β-protons of the aromatic residue and its associated ring protons (Wagner and Wüthrich, 1992; Billeter et al., 1982; Wüthrich, 1986). Sometimes it may however be difficult to obtain complete assignments because of a high density of NOEs, as mentioned above, and/or a poor dispersion of ^{1}H chemical shifts. In general, pulse sequences which exclusively rely on the transfer of magnetization via one-bond scalar couplings reduce the ambiguities considerably. However, experiments such as HCCH-COSY (Kay et al., 1990) or HCCH-TOCSY (Fesik et al., 1990; Bax et al., 1990) are not designed for a transfer between the β- and γ-carbon spins of aromatic side-chains. In a pioneering work, Yamazaki et al. (1993) introduced the (Hβ)Cβ(CγCδ)Hδ and (Hβ)Cβ(CγCδCε)Hε experiments which correlate $^{13}C^{\beta}$ with aromatic ^{1}H chemical shifts via multiple-

*To whom correspondence should be addressed. E-mail: murph@bpc.uni-frankfurt.de

relay sequences. Pulse sequences employing different mixing schemes have also been successfully applied to obtain similar correlations (Grzesiek and Bax, 1995; Carlomagno et al., 1996). In a different approach, connectivities between aromatic and aliphatic resonances can be established via common correlations to γ-carbons in a combination of at least two distinct experiments (Löhr and Rüterjans, 1996; Prompers et al., 1998). The latter strategy benefits from the good dispersion of $^{13}C^{\gamma}$ chemical shifts in aromatic amino acid residues. With increasing size of the protein, however, most of these schemes tend to become less efficient, primarily due to relatively fast transverse relaxation of $^{1}H^{\beta}/^{13}C^{\beta}$ coherences. Moreover, in highly deuterated proteins neither the NOE- nor the known ^{1}J-based methods are able to provide intraresidual connectivites to assign exchangeable side-chain protons in histidine or tryptophan residues.

This article describes new pulse sequences to selectively link $^{13}C^{\beta}$ chemical shifts to $^{1}H^{\delta 2}/^{13}C^{\delta 2}$ of histidines in $^{13}C/^{15}N$-labelled proteins and to $^{1}H^{\varepsilon 1}/^{15}N^{\varepsilon 1}$ of tryptophanes in $^{13}C/^{15}N$- or $^{2}H/^{13}C/^{15}N$-labelled proteins. Both experiments are of the 'out-and-back' type with magnetization starting off from aromatic spins. This enables the constructive use of dipole-dipole (DD)-chemical shift anisotropy (CSA) relaxation interference via [^{13}C, ^{1}H]-TROSY (Pervushin et al., 1998a) and [^{15}N, ^{1}H]-TROSY (Pervushin et al., 1997) schemes, respectively, making possible their application to relatively large proteins.

Materials and methods

Sample preparations

Uniformly $^{13}C/^{15}N$ labelled recombinant DFPase from *Loligo vulgaris* was expressed in *E. coli* grown on M9 minimal medium containing 1 g l^{-1} $^{15}NH_4Cl$ (99%) (Martek Biosciences Corp., Columbia, MD) as the sole nitrogen source and 1 g l^{-1} $^{13}C_6$ glucose (>98%) (Martek) as well as 2.5 g l^{-1} $^{13}C_3$ glycerol (99%) (Martek) as carbon sources. Triply labelled DFPase was produced using a $^{2}H/^{13}C/^{15}N$-enriched (>96%) algal lysate based medium (Cambridge Isotope Laboratories, Inc., Andover, MA) in 99.9% D_2O, supplemented with 1 g l^{-1} $^{2}H_7/^{13}C_6$ glucose (>97%) (Martek) and 1 g l^{-1} $^{15}NH_4Cl$. The sequence was encoded in the pKKHisND plasmid as a fusion to a cleavable N-terminal His-tag. The protocol for protein purification was reported elsewhere (Hartleib and Rüterjans, 2001). Samples were dissolved in 10 mM 1,3-bis[tris-(hydroxymethyl-) methylamino]-propane (Bis-Tris-propane) buffer, pH = 6.5, containing 5 mM $CaCl_2$.

Recombinant familiy 11 xylanase from *Bacillus agaradhaerens* was expressed in *E. coli* carrying the pET-3a plasmid, encoding for residues 1-207. $^{13}C/^{15}N$ enrichment was achieved by growing cells on M9 minimal medium supplemented with 1 g l^{-1} $^{13}C_6$ glucose, 2.5 g l^{-1} $^{13}C_3$ glycerol and 1 g l^{-1} $^{15}NH_4Cl$. The purification is analogous to the procedure of Sabini et al. (1999). The pH was adjusted to 5.3 in 10 mM sodium acetate buffer.

Protein concentrations of $^{13}C/^{15}N$-labelled DFPase, $^{2}H/^{13}C/^{15}N$-labelled DFPase and $^{13}C/^{15}N$-labelled xylanase samples were 1.6 mM, 0.75 mM and 1.5 mM, respectively. All buffers contained 5% D_2O, 0.03% NaN_3 and 50 μg/ml Pefabloc protease inhibitor as well as 0.15 mM 3-(trimethylsilyl)-1-propanesulfonic acid (DSS) as internal standard. Samples were placed in Shigemi microcells with total volumes ranging from 300 to 350 μl.

Description of the pulse sequences

The [^{13}C, ^{1}H]-TROSY-HCD(CG)CB sequence depicted in Figure 1 is derived from the H(CD)CGCB experiment, described previously (Löhr and Rüterjans, 1996), with delay durations optimized to selectively observe correlations within histidine side-chains. Further modifications include the combined use of ^{1}H and ^{13}C steady-state polarizations followed by selection of the slowly relaxing ^{1}H-coupled ^{13}C magnetization component in a TROSY fashion (Pervushin et al., 1998a; Brutscher et al., 1998), gradient coherence selection and artifact suppression and the replacement of a $^{13}C^{\gamma}$ by a $^{13}C^{\delta}$ chemical shift evolution period.

In more detail, after the initial INEPT (Morris and Freeman, 1978) transfer, δ-carbon coherence of histidines evolves into antiphase magnetization with respect to its neighbouring carbon spin during period Δ which is tuned to $1/(2^{1}J_{C\delta C\gamma})$. The following ^{13}C 90° pulse then creates antiphase magnetization on γ-carbons, where it resides for a total duration of $2\varepsilon + 2\zeta$, amounting to $2/^{1}J_{C\delta C\gamma}$. This time is exploited for recording $^{13}C^{\beta}$ chemical shifts in an HMQC (Bax et al., 1983, Bendall et al., 1983) fashion. As the time required for de- and rephasing of the scalar $^{13}C^{\gamma}$-$^{13}C^{\beta}$ interaction ($\zeta \approx 1/2^{1}J_{C\gamma C\beta}$)) is shorter than $2/^{1}J_{C\delta C\gamma}$, two compensating delays ε have been introduced, each containing a $^{13}C^{\beta}$ refocusing pulse in its centre. These periods are decremented as a function

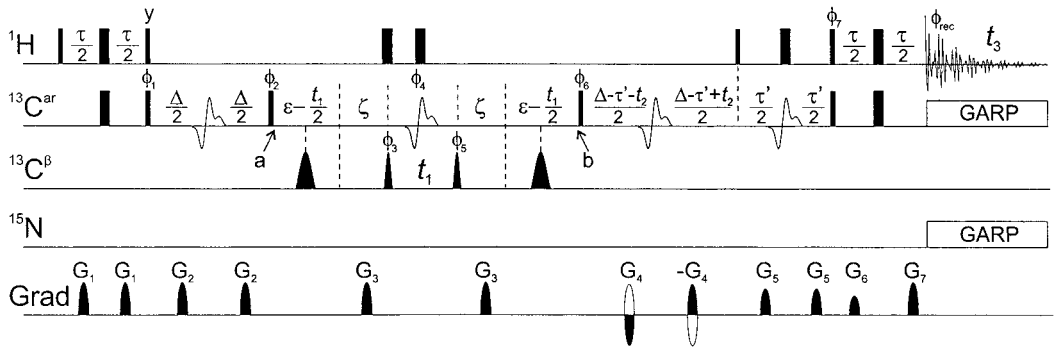

Figure 1. Pulse sequence of the 3D [^{13}C, ^{1}H]-TROSY-HCD(CG)CB experiment for the correlation of aromatic $^{1}H^{\delta 2}$-$^{13}C^{\delta 2}$ with aliphatic $^{13}C^{\beta}$ resonances in histidine side-chains. Proton, carbon and nitrogen carrier frequencies are centered at the water (4.75 ppm), the histidine $^{13}C^{\beta}$ region (32.5 ppm) and the imidazole ^{15}N region (197 ppm), respectively. Pulses on aromatic carbons are applied at 128 ppm using phase modulation (Boyd and Soffe, 1989; Patt, 1992). Immediately before acquisition the ^{13}C carrier is switched to the aromatic region (120 ppm). Narrow and wide filled bars denote rectangular 90° and 180° pulses, respectively, applied with RF field strengths of 28.0 kHz for protons and 17.8 kHz for carbons. The shaped 180° $^{13}C^{ar}$ pulses are G^3 Gaussian cascades (Emsley and Bodenhausen, 1990) with a duration of 270 μs (220 μs) for application at 500 MHz (600 MHz) spectrometers. 90° and 180° pulses on β-carbons have the shape of the centre lobe of a sin(x)/x function and widths of 150 μs. Heteronuclear decoupling during acquisition is achieved with GARP-1 (Shaka et al., 1985) modulations of 1.25 kHz (^{13}C, 500 MHz spectrometer), 0.83 kHz (^{15}N, 500 MHz), 1.67 kHz (^{13}C, 600 MHz) and 1.0 kHz (^{15}N 600 MHz). Fixed delays are adjusted as follows: $\tau = 2.2$ ms, $\Delta = 6.6$ ms, $\varepsilon = 4.8$ ms, $\zeta = 8.8$ ms, $\tau' = 2.4$ ms. Unless specified, pulses are applied along the x-axis. Phase cycling is: $\phi_1 = 2(x), 2(-x)$; $\phi_2 = 8(y), 8(-y)$; $\phi_3 = x, -x$; $\phi_4 = 2(x), 2(-x), 2(y), 2(-y)$; $\phi_5 = 8(x), 8(-x)$; $\phi_6 = y, -y$; $\phi_7 = y$; $\phi_{rec} = R, 2(-R), R$, where $R = x, 2(-x), x$. Quadrature in t_1 is achieved by altering ϕ_3 in the States-TPPI (Marion et al., 1989) manner. The phase of the second proton 90° pulse is adjusted for a Bruker Avance spectrometer to constructively add components originating from ^{1}H and ^{13}C steady-state magnetizations (Pervushin et al., 1998a; Brutscher et al., 1998). On other spectrometer types phase inversion of the latter pulse may be required for the same purpose. Pulsed field gradients are sine-bell shaped and have the following durations, peak amplitudes and directions: G_1, 0.4 ms, 5 G cm^{-1}, x; G_2, 0.4 ms, 5 G cm^{-1}, y; G_3, 0.4 ms, 7.5 G cm^{-1}, x; G_4, 0.5 ms, −35 G cm^{-1}, xyz; G_5, 0.3 ms, 4 G cm^{-1}, xy; G_6, 0.5 ms, 3.5 G cm^{-1}, xyz, G_7, 0.5 ms, 21.1 G cm^{-1}, xyz. N- and P-type coherences are collected alternately by inverting the polarity of G_4 along with the pulse phase ϕ_7. The two transients are stored separately and then added and subtracted to form the real and imaginary parts of a complex interferogram with a 90° zero-order phase shift being added to one of the components.

of t_1 in order to keep the overall duration of transverse $^{13}C^{\gamma}$ magnetization constant, thus avoiding $^{13}C^{\beta}$ line broadening along the multiple-quantum ω_1 domain due to the large scalar $^{13}C^{\gamma}$-$^{13}C^{\delta}$ and $^{13}C^{\gamma}$-$^{13}C^{\beta}$ couplings. Note that the period $2\varepsilon + 2\zeta$ almost exactly matches $3/(2^1J_{CC})$ in aromatic spin systems of other amino acid residues such that $^{13}C^{\gamma}$ in-phase magnetization evolves in the latter, which is not converted into observable coherences before acquisition. As a consequence, the [^{13}C, ^{1}H]-TROSY-HCD(CG)CB sequence exclusively provides correlations within histidine side-chains.

Since proton pulses are not applied during the Δ and $\Delta - \tau'$ periods, a partial cancellation of ^{1}H-^{13}C dipole-dipole and ^{13}C chemical shift anisotropy (CSA) interactions leads to an attenuated transverse relaxation of aromatic carbon coherences (Pervushin et al., 1998a). In contrast, a proton 180° pulse is needed to refocus the $^{1}J_{H\beta C\beta}$ interaction during t_1. Its effect on aromatic carbons is, however, negated by the application of a second 180° pulse (Fiala et al., 2000; Yan et al., 2000; Löhr et al., 2000; Eletsky et al., 2001) just prior to the evolution time. The slowly relaxing highfield ^{13}C doublet component is selected by a spin-state-selective coherence transfer (S^3CT) (Meissner and Sørensen, 1999) to δ-protons which are finally detected. During acquisition, ^{13}C decoupling is applied because the small CSA of aromatic protons precludes efficient line-narrowing due to cross-correlated relaxation (Pervushin et al., 1998a). Optional ^{15}N decoupling removes the unresolved long-range J couplings to imidazole nitrogens. Frequency labelling of δ-carbons (t_2) is implemented in a constant-time (Bax and Freeman, 1981) manner during the $^{13}C^{\gamma} \rightarrow {}^{13}C^{\delta}$ back-transfer period. If the experiment is run as a two-dimensional H(CDCG)CB version, a slightly enhanced sensitivity may be obtained by replacing the S^3CT element by a simple ^{1}H 90° pulse, thus superimposing the $^{13}C^{\delta}$ TROSY and anti-TROSY components (Riek et al., 2001).

The [^{15}N, ^{1}H]-TROSY-HN(CDCG)CB pulse scheme outlined in Figure 2 comprises four successive steps to transfer magnetization from the exchangeable tryptophan ε1-proton to the intraresidual β-carbon via $^{1}H^{\varepsilon 1}$-$^{15}N^{\varepsilon 1}$, $^{15}N^{\varepsilon 1}$-$^{13}C^{\delta 1}$, $^{13}C^{\delta 1}$-$^{13}C^{\gamma}$ and $^{13}C^{\gamma}$-$^{13}C^{\beta}$ one-bond couplings. During the period η, required

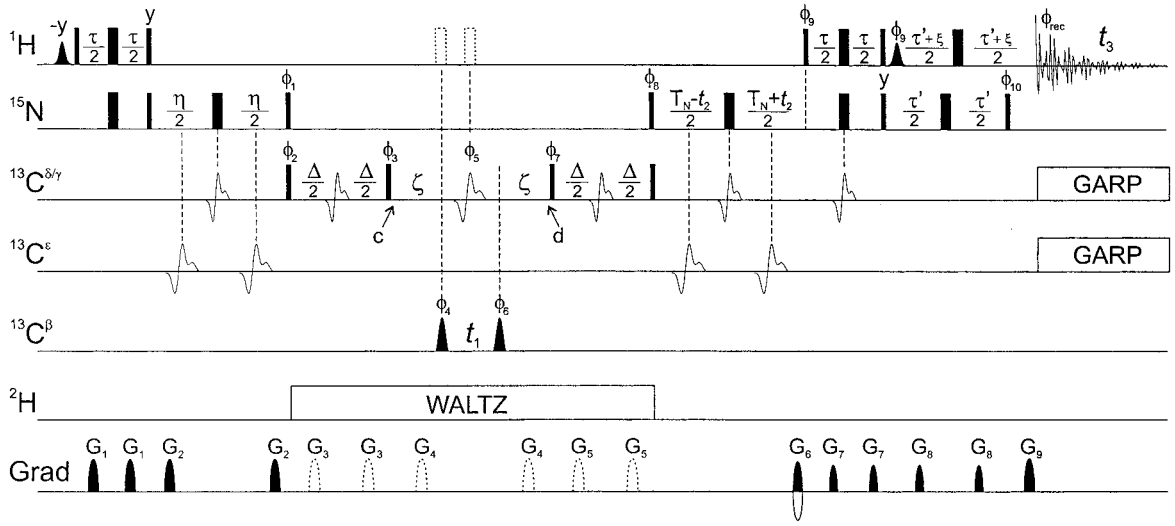

Figure 2. [^{15}N, ^{1}H]-TROSY-HN(CDCG)CB pulse scheme to correlate indole $^{1}H^{\varepsilon 1}/^{15}N^{\varepsilon 1}$ with $^{13}C^{\beta}$ resonances in tryptophan side-chains. Carrier offsets are 4.75 ppm (^{1}H), 130.5 ppm (^{15}N), 31.5 ppm (^{13}C) and 5.0 ppm (^{2}H). Prior to acquisition the ^{13}C carrier frequency is shifted to 132 ppm. RF field strengths for rectangular ^{1}H, ^{15}N and ^{13}C pulses are 28.0, 7.7 and 17.8 kHz, respectively, while the power level is reduced to 1.67 kHz for ^{13}C GARP decoupling. Selective water-flip-back pulses have a Gaussian shape, truncated at 10%, and a duration of 2.1 ms. The sinc-shaped 90° $^{13}C^{\beta}$ pulses have a width of 150 μs. Phase modulated off-resonance pulses on aromatic $^{13}C^{\delta/\gamma}$ and $^{13}C^{\varepsilon}$ nuclei are applied at 119 and 139.5 ppm, respectively, with the exception of the $^{13}C^{\gamma}$-selective G^3 pulse in the centre of the t_1 evolution time, which is applied at 110.5 ppm. The duration of the latter pulse is 1.7 ms (1.5 ms) for applications at 500 MHz (600 MHz) spectrometers, whereas G^3 pulses centered in periods Δ and ε have a width of 400 μs (350 μs) and the width of G^3-shaped $^{13}C^{\varepsilon}$-selective inversion pulses is adjusted to 3 ms (2.5 ms). Deuterium decoupling is achieved with a WALTZ-16 sequence (Shaka et al., 1983) applied with an RF field strength of 0.8 kHz. Pulses and gradients indicated by dashed contours are omitted for applications to deuterated proteins, whereas ^{2}H decoupling is unnecessary for non-deuterated proteins. Delay durations are: $\tau = 4.6$ ms, $\eta = 26$ ms, $\Delta = 6.4$ ms, $\zeta = 8.5$ ms, $T_N = \eta - \tau$, $\tau' = 5.4$ ms, $\xi = 0.4$ ms. The default pulse phase is x. Phases are cycled according to $\phi_1 = 2(y), 2(-y)$; $\phi_2 = 8(x), 8(-x)$; $\phi_3 = 2(y), 2(-y)$; $\phi_4 = x, -x$; $\phi_5 = 4(x), 4(y), 4(-x), 4(-y)$; $\phi_6 = 16(x), 16(-x)$; $\phi_7 = 32(y), 32(-y)$; $\phi_8 = 32(x), 32(-x)$; $\phi_9 = y$; $\phi_{10} = x$; $\phi_{rec} = R, 2(-R), R, 2[-R, 2(R), -R], R, 2(-R), R$, with $R = x, 2(-x), x$. Sign discrimination in the ω_1 dimension is accomplished by States-TPPI of phase ϕ_4. The phases of the first selective and the second unselective 90° proton pulses are valid for Bruker Avance spectrometers, whereas for other spectrometer types they may have to be inverted to constructively add native ^{1}H and ^{15}N magnetizations (Pervushin et al. 1997; Zhu et al., 1998). Sine-bell shaped gradients are applied with the following lengths, peak amplitudes and directions: G_1, 0.5 ms, 5 G cm^{-1}, x; G_2, 0.5 ms, 5 G cm^{-1}, y; G_3, 0.5 ms, 6 G cm^{-1}, x; G_4, 0.5 ms, 5 G cm^{-1}, y; G_5, 0.5 ms, 7.5 G cm^{-1}, x; G_6, 1.6 ms, 19.73 G cm^{-1}, xyz; G_7, 0.3 ms, 4 G cm^{-1}, xy; G_8, 0.3 ms, 5.5 G cm^{-1}, xy; G_9, 0.2 ms, 16 G cm^{-1}, xyz. Echo- and antiecho coherence transfer pathways are acquired alternately by inversion of the duration of gradient G_6 and pulse phases ϕ_9 and ϕ_{10}. Axial peaks are shifted to the edge of the spectrum in the ^{15}N dimension by inverting ϕ_8 and the receiver phase in every other t_2 increment.

for the $^{15}N^{\varepsilon 1}$-$^{13}C^{\delta 1}$ transfer, it is essential to refocus the $^{1}J_{N\varepsilon 1C\varepsilon 2}$ interaction by selective 180° pulses on $^{13}C^{\varepsilon 2}$ to avoid a leakage of magnetization, otherwise leading to a substantial loss of sensitivity. As in the HCD(CG)CB sequence, the magnetization is subsequently passed to γ-carbons in a CC-Relay step with Δ adjusted to $1/(2^{1}J_{C\delta 1C\gamma})$, and then frequency labelled with $^{13}C^{\beta}$ chemical shifts, employing a $^{13}C^{\gamma}$-$^{13}C^{\beta}$ HMQC module. However, in contrast to histidine imidazole rings, the $^{13}C^{\gamma}$ spin of indole ring systems has a second aromatic $^{1}J_{CC}$ coupling partner. As the size of the two $^{13}C^{\gamma}$-$^{13}C^{\delta}$ coupling constants differs significantly ($^{1}J_{C\gamma C\delta 1} \approx 72$ Hz, $^{1}J_{C\gamma C\delta 2} \approx 55$ Hz) it is impossible to find a reasonable value for the total duration of the HMQC element, which would correspond to multiples of the inverse of both $^{1}J_{CC}$ coupling constants. Instead, modulations by aromatic $^{1}J_{CC}$ interactions are avoided by applying a $^{13}C^{\gamma}$-selective 180° pulse in the centre of t_1. This is possible because tryptophan $^{13}C^{\gamma}$ resonances are usually well separated from those of other aromatic carbons. Finally, the magnetization is transferred back to ε1-protons via the reverse pathway, using a sensitivity enhanced [^{15}N, ^{1}H]-TROSY detection scheme (Czisch and Boelens, 1998; Andersson et al., 1998; Pervushin et al., 1998b; Zhu et al., 1998; Weigelt, 1998; Rance et al., 1999) to attenuate transverse nitrogen and proton relaxation. In the present implementation, gradient echo/antiecho coherence selection is employed with a minimized number of ^{1}H 180° pulses (Dingley and Grzesiek, 1998; Loria et al., 1999). The final 180° pulse on $^{13}C^{\delta/\gamma}$ concatenates the τ period

of the single transition-to-single transition polarization transfer (ST2-PT) with the $^{13}C^{\delta} \rightarrow ^{15}N$ back transfer (Loria et al., 1999; Salzmann et al., 1999a). Water-flip back pulses are applied in the usual manner (Grzesiek and Bax, 1993, Stonehouse et al., 1994, Matsuo et al., 1996) to ensure a minimal saturation of fast exchanging indole NH protons. During acquisition, decoupling of aromatic carbons should be applied, resulting in purely absorptive lineshapes and a slightly enhanced sensitivity (Yang and Kay, 1999).

If the sequence is applied to deuterated protein samples, ^{2}H decoupling is mandatory during periods of transverse ^{13}C magnetization to eliminate the effect of the deuterium quadrupolar interaction (Grzesiek et al., 1993), otherwise causing an accelerated decay of ^{13}C coherences. In applications to non-deuterated proteins, the sequence also allows for ^{1}H-$^{13}C^{ar}$ DD/$^{13}C^{ar}$ CSA cross correlation during the two Δ periods, thus taking advantage of both [^{15}N, ^{1}H]- and [^{13}C, ^{1}H]-TROSY effects.

A modified version of the [^{15}N, ^{1}H]-TROSY-HN(CDCG)CB sequence can be used to correlate histidine β-carbon resonances with nitrogen bound imidazole protons, provided that the latter exchange sufficiently slow with the solvent. For this purpose, the pulses and delays between time points a and b in the scheme of Figure 1 substitute for those between points c and d in Figure 2. Obviously, for applications to $^{2}H/^{13}C/^{15}N$-labelled samples, deuterium has to be decoupled during t_1 whereas the two proton 180° pulses are omitted. In this experiment, the flow of magnetization is $^{1}H^{N\varepsilon 2} \rightarrow ^{15}N^{\varepsilon 2} \rightarrow ^{13}C^{\delta 2} \rightarrow ^{13}C^{\gamma} \rightarrow ^{13}C^{\beta}(t_1) \rightarrow ^{13}C^{\gamma} \rightarrow ^{13}C^{\delta 2} \rightarrow ^{15}N^{\varepsilon 2}(t2) \rightarrow ^{1}H^{N\varepsilon 2}$. In cases where $^{1}H^{N\delta 2}$ rather than $^{1}HN^{N\varepsilon 2}$ resonances are observable, the two Δ periods flanking the $^{13}C^{\gamma}$-$^{13}C^{\beta}$ HMQC part would have to be omitted to obtain the following pathway: $^{1}H^{N\delta 1} \rightarrow ^{15}N^{\delta 1} \rightarrow ^{13}C^{\gamma} \rightarrow ^{13}C^{\beta}(t_1) \rightarrow ^{13}C^{\gamma} \rightarrow ^{15}N^{\delta 1}(t2) \rightarrow ^{1}H^{N\delta 1}(t_3)$.

Chemical shifts of aromatic carbons adjacent to indole and possibly imidazole nitrogens can be assigned in a [^{15}N, ^{1}H]-TROSY-HNC^{ar} experiment. The pulse sequence (not shown) is basically identical with those of HNCA or HNCO experiments (Ikura et al., 1990; Salzmann et al., 1998), except that the ^{13}C carrier is positioned in the aromatic region. Due to the presence of two relatively large $^{1}J_{NCar}$ and additional long-range interactions in these ring systems, the optimal length of the ^{15}N-^{13}C de- and rephasing delays η is as short as 15–17 ms. In a similar manner, γ-carbon chemical shifts of tryptophan residues can be

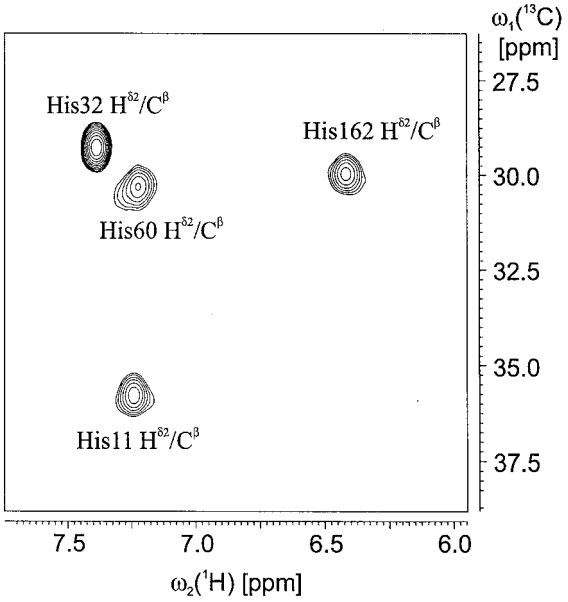

Figure 3. Two-dimensional [^{13}C, ^{1}H]-TROSY-H(CDCG)CB spectrum of xylanase recorded at a proton frequency of 500 MHz. Sequential assignments of aromatic protons are based on correlations of $^{1}H^{\delta 2}$ with previously determined $^{13}C^{\beta}$ resonances.

sampled after inserting a CC-Relay step and ensuring that the $^{1}J_{N\varepsilon 1C\varepsilon 2}$ coupling is not active during the $N^{\varepsilon 1}$-$C^{\delta 1}$ magnetization transfer. The resulting [^{15}N, ^{1}H]-TROSY-HN(CD)CG pulse sequence (not shown) is reminiscent of the HNCACB sequence (Wittekind and Mueller, 1993; Salzmann et al., 1999b) and can be derived from the [^{15}N, ^{1}H]-TROSY-HN(CDCG)CB scheme of Figure 2 by replacing the section between time points c and d by an incremented delay t_1.

Data acquisition and processing

Spectra were recorded with xylanase and DFPase samples at ^{1}H Larmor frequencies of 499.87 and 600.13 MHz, respectively, using Bruker Avance spectrometers equipped with 5 mm $^{1}H\{^{13}C/^{15}N\}$ three-axis gradient triple resonance probes. The temperature setting was 28 °C in all experiments.

A three-dimensional [^{13}C, ^{1}H]-TROSY-HCD(CG)CB spectrum was acquired on doubly-labelled DFPase using spectral widths of 14.0 ppm ($^{13}C^{\beta}$, ω_1), 21.5 ppm ($^{13}C^{\delta}$, ω_2) and 8.4 ppm ($^{1}H^{\delta}$, ω_3). Signals were aliased four times in ω_2, such that the apparent carrier position in this dimension was 118.5 ppm. Time domain data consisted of 16 × 10 × 256 complex points, corresponding to acquisition times of 7.5, 3.1 and 50.8 ms in t_1, t_2 and t_3, respectively. Accu-

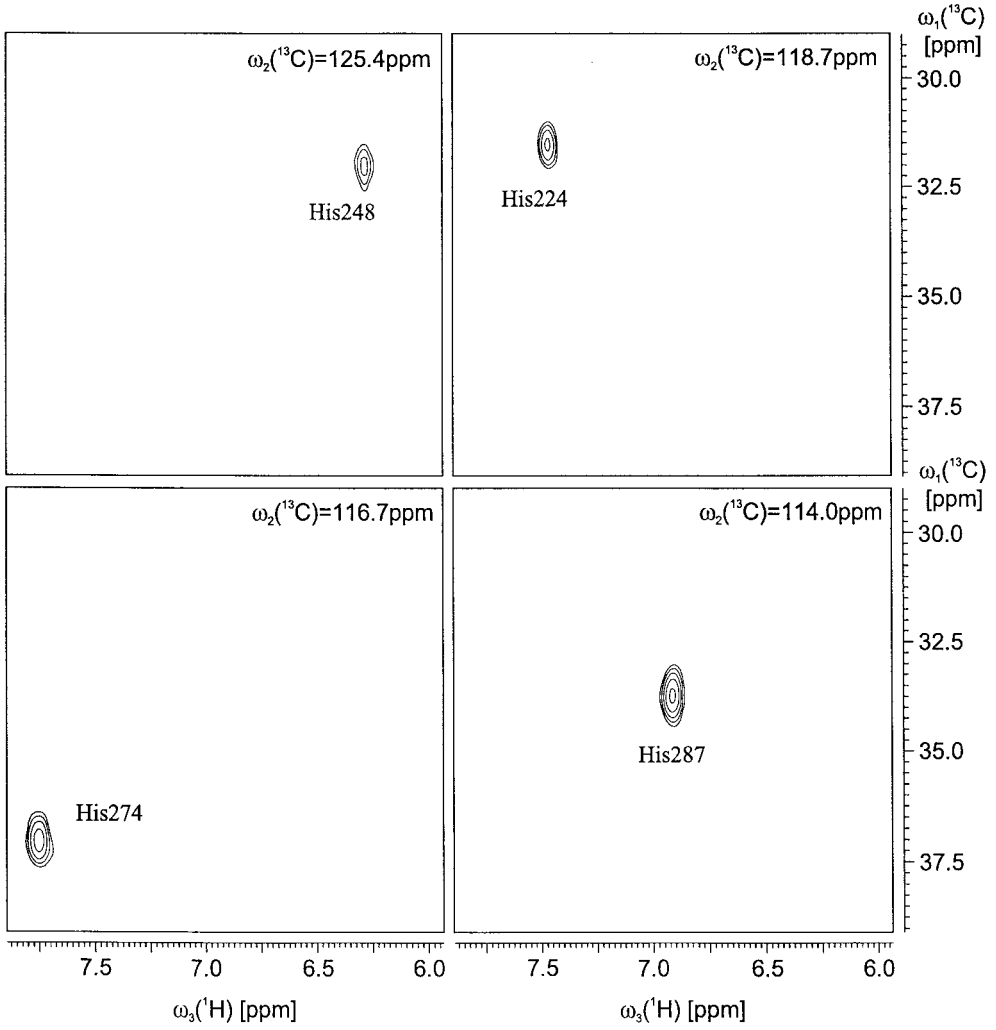

Figure 4. Expansions from ω_1/ω_3 planes of a 3D [^{13}C, ^{1}H]-TROSY-HCD(CG)CB spectrum of DFPase, taken at the $^{13}C^{\delta 2}$ chemical shifts given in the upper right corners. The experiment was carried out at 600 MHz using a $^{13}C/^{15}N$-labelled sample.

mulation of 64 scans per FID resulted in a measuring time of 13 h. For xylanase, the experiment was carried out as a two-dimensional ($^{1}H^{\delta}$-$^{13}C^{\beta}$) version by setting $t_2 = 0$ in the pulse sequence of Figure 1. Spectral widths were 12.4 ppm in the $^{13}C^{\beta}$ and 6.5 ppm in the $^{1}H^{\delta}$ dimension. The spectrum was recorded within 20 minutes using 32 scans per FID and 16 complex increments of 192 complex points, corresponding to acquisition times of 9.6 ms (t_1) and 59.0 ms (t_2).

The [^{15}N, ^{1}H]-TROSY-HN(CDCG)CB experiment of Figure 2 was carried out on $^{2}H/^{13}C/^{15}N$-labelled DFPase with $t_2 = 0$ to provide a two-dimensional ($^{1}H^{N\varepsilon 1}$-$^{13}C^{\beta}$) correlation spectrum. Spectral widths comprised 11.8 ppm and 17.1 ppm in the $^{13}C^{\beta}$ and $^{1}H^{N\varepsilon 1}$ dimensions with acquisition times (number of complex points) of 12.3 ms (22) and 75.0 ms (768), respectively. For each FID 128 transients were accumulated, yielding a measuring time of 4 h. A three-dimensional [^{15}N, ^{1}H]-TROSY-HN(CDCG)CB experiment was performed for xylanase with spectral widths of 11.8 ppm, 11.4 ppm and 16.0 ppm in the $^{13}C^{\beta}$ (ω_1), $^{15}N^{\varepsilon 1}$ (ω_2) and $^{1}H^{N\varepsilon 1}$ (ω_3), dimension, respectively. Within 14 h, the spectrum was recorded with 64 scans per FID and acquisition times of 10.8 ms (t_1, 16 complex points), 17.2 ms (t_2, 10 complex points) and 64.0 ms (t_3, 512 complex points). The [^{15}N, ^{1}H]-TROSY-HN(CDCG)CB variant adapted for histidine side-chains was applied to the triply-labelled DFPase sample as a two-dimensional experiment with acquisition times of 9.7 ms (23 com-

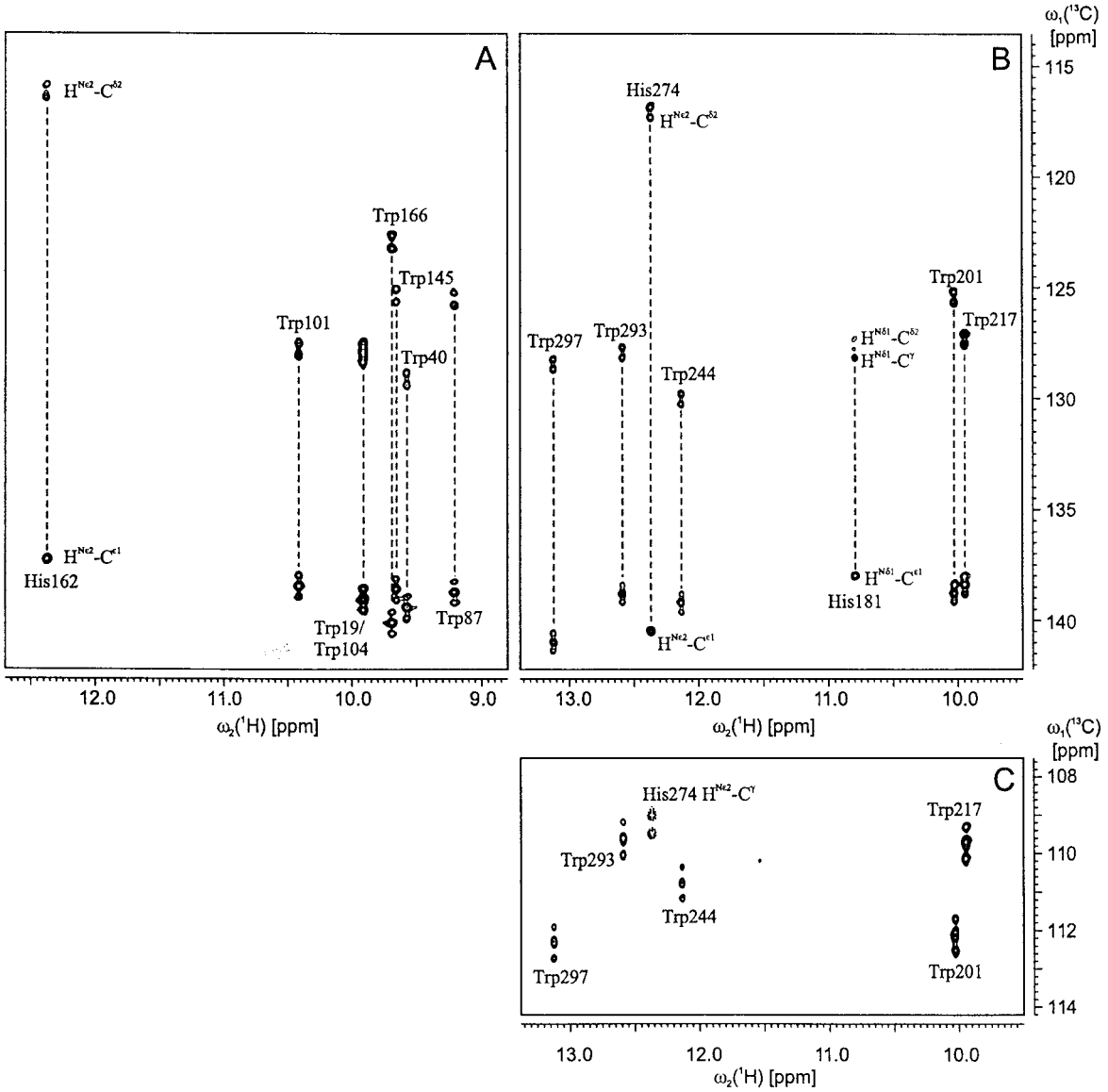

Figure 5. Determination of $^{13}C^{\varepsilon2}$, $^{13}C^{\delta1}$ and $^{13}C^{\gamma}$ chemical shifts in tryptophan side-chains: (A) 2D [^{15}N, ^1H]-TROSY-H(N)C^{ar} spectrum of $^{13}C/^{15}N$-labelled xylanase, recorded at 500 MHz, (B) [^{15}N, ^1H]-TROSY-H(N)C^{ar} and (C) 2D [^{15}N, ^1H]-TROSY-H(NCD)CG spectra of $^2H/^{13}C/^{15}N$-labelled DFPase, recorded at 600 MHz. Cross peaks from histidine residues, also appearing in the [^{15}N, ^1H]- TROSY -H(N)car spectra (A and B), are designated explicitly. For tryptophanes, ^{13}C upfield and downfield cross peaks always correspond to δ1- and ε2-carbons, respectively. $^1H^{N\varepsilon1}$ and $^{13}C^{\varepsilon}2$ chemical shifts of Trp19 and Trp104 in xylanase exhibit complete degeneracy. In the spectrum of part C, showing $^1H^{N\varepsilon1}$-$^{13}C^{\gamma}$ correlations in tryptophan residues, positive and negative contours are drawn with solid and broken lines, respectively. The aliased His274 cross peak appears negative due to a 180° first order phase correction in the carbon dimension.

plex points) in the $^{13}C^{\beta}$ and 75.0 ms (768 complex points) in the $^1H^{N\varepsilon2}$ dimension and spectral widths adjusted to 15.8 ppm and 17.1 ppm, respectively. The measurement time was 4 h, using 128 scans per FID.

Two-dimensional [^{15}N, ^1H]-TROSY-H(N)C^{ar} experiments have been executed for $^2H/^{13}C/^{15}N$-labelled DFPase with $\eta = 15$ ms and for $^{13}C/^{15}N$-labelled xylanase with $\eta = 17$ ms. Spectral widths were adjusted to 36.8 ppm (^{13}C) and 17.1 ppm ($^1H^N$) for DFPase and to 29.0 ppm (^{13}C) and 16.2 ppm ($^1H^N$) for xylanase. Acquisition times (number of complex points) were 21.6 ms (120, t_1) and 56.2 ms (576, t_2) for DFPase and 34.8 ms (128, t_2) and 63.3 ms (512, t_1) for xylanase. For each spectrum, 32 scans were accumu-

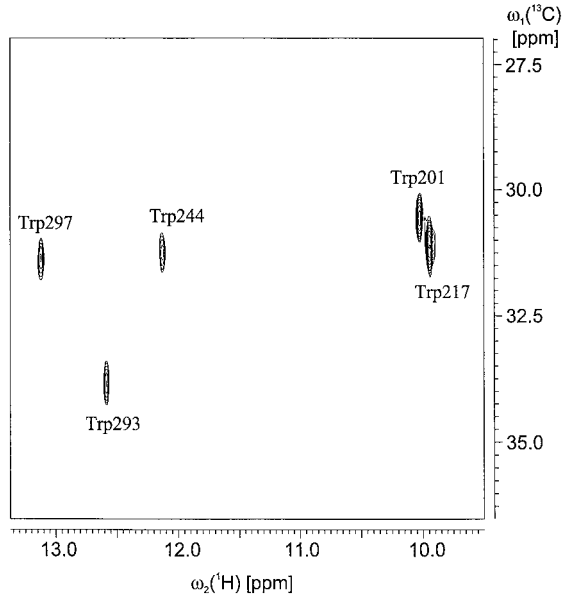

Figure 6. Expansion from a 600 MHz 2D [^{15}N, ^{1}H]-TROSY-H(NCDCG)CB spectrum of ^{2}H/^{13}C/^{15}N-labelled DFPase recorded with the pulse sequence of Figure 2 with t_2 set to 0. Each cross peak links a tryptophan indole $^{1}H^{\varepsilon 1}$ resonance with the $^{13}C^{\beta}$ chemical shift of the same side-chain. Note the absence of cross peaks for histidine residues.

lated per FID, giving rise to measuring times of 4.5 h (DFPase) and 3 h (xylanase). A two-dimensional [^{15}N, ^{1}H]-TROSY-H(NCD)CG spectrum was recorded on the ^{2}H/^{13}C/^{15}N-labelled DFPase sample with spectral widths comprising 30.1 ppm (^{13}C) and 17.1 ppm ($^{1}H^{N}$). Time domain data consisted of 160 × 576 complex points, corresponding to acquisition times of 35.2 and 56.2 ms in t_1 and t_2, respectively. The spectrum was acquired within 10 h using 64 scans per increment.

Spectra were processed using Bruker XWINNMR software. Linear prediction was applied in indirectly detected dimensions to extend time domain data. In the carbon dimension of [^{15}N, ^{1}H]-TROSY-HN(CDCG)CB experiments for the assignment of tryptophan resonances, acquisition was delayed by three dwell-times due to the relatively long selective $^{13}C^{\gamma}$ pulse in the centre of t_1. In order to avoid first order phase corrections, the missing first points were constructed by linear prediction. Prior to Fourier transformation and zero-filling, data were apodized with squared-cosine weighting functions in all dimensions. To assess the sensitivity of the experiments, contour levels of all spectra displayed in the following are plotted on an exponential scale using a factor of $2^{1/2}$.

Results and discussion

The utility of the above described pulse sequences was tested with two proteins of different sizes. The medium-sized protein xylanase from *Bacillus agaradhaerens* consists of 207 amino acid residues (MW 23 kDa), seven of which are tryptophans and four of which are histidines. As an example for a larger protein, diisopropylfluorophosphatase (DFPase) from *Loligo vulgaris* (314 residues, MW 35 kDa) was chosen, which contains six tryptophan and histidine residues each. Both proteins were uniformly ^{13}C/^{15}N-labelled, while DFPase was available as a protonated and a perdeuterated sample.

Figure 3 shows a 2D [^{13}C, ^{1}H]-TROSY-H(CDCG)CB spectrum of xylanase containing $^{1}H^{\delta 2}$-$^{13}C^{\beta}$ correlations for each of the four histidines. Sequence-specific assignment of β-carbon chemical shifts, available from standard triple-resonance experiments such as HNCACB (Wittekind and Mueller, 1993) or CBCA(CO)NH (Grzesiek and Bax, 1992), are thus unambiguously transferred into the aromatic ring system. The fact that the data acquisition required a time as short as 20 min demonstrates the high sensitivity of the method. Difficulties due to the near-degeneracy of the δ2-proton resonances of His11 and His60 might be overcome in the three-dimensional version of the experiment, where the associated δ-carbon chemical shifts are resolved.

When applied to DFPase, the efficiency of the [^{13}C, ^{1}H]-TROSY-HCD(CG)CB experiment was diminished considerably. This is a consequence of the shorter ^{1}H and ^{13}C transverse relaxation times compared to xylanase. It should be noted that the TROSY-type enhancement is active for δ-carbons (periods Δ in the pulse sequence of Figure 1), but not in the ≈27 ms period where transverse magnetization resides with unprotonated γ-carbons. Since the total accumulation time of the [^{13}C, ^{1}H]-TROSY-HCD(CG)CB experiment for DFPase was determined by sensitivity rather than the number increments or phase cycling, it was advantageous to record it in a three-dimensional version, to obtain additional $^{13}C^{\delta 2}$ chemical shift information and gain resolution. Owing to the echo/antiecho-type quadrature detection and its constant-time character the third dimension can be introduced without any loss of sensitivity. Imidazole resonance assignments of four out of the six histidine residues of DFPase as derived from the 3D [^{13}C, ^{1}H]-TROSY-HCD(CG)CB spectrum, are presented in Figure 4. The assignment of His219 followed from a

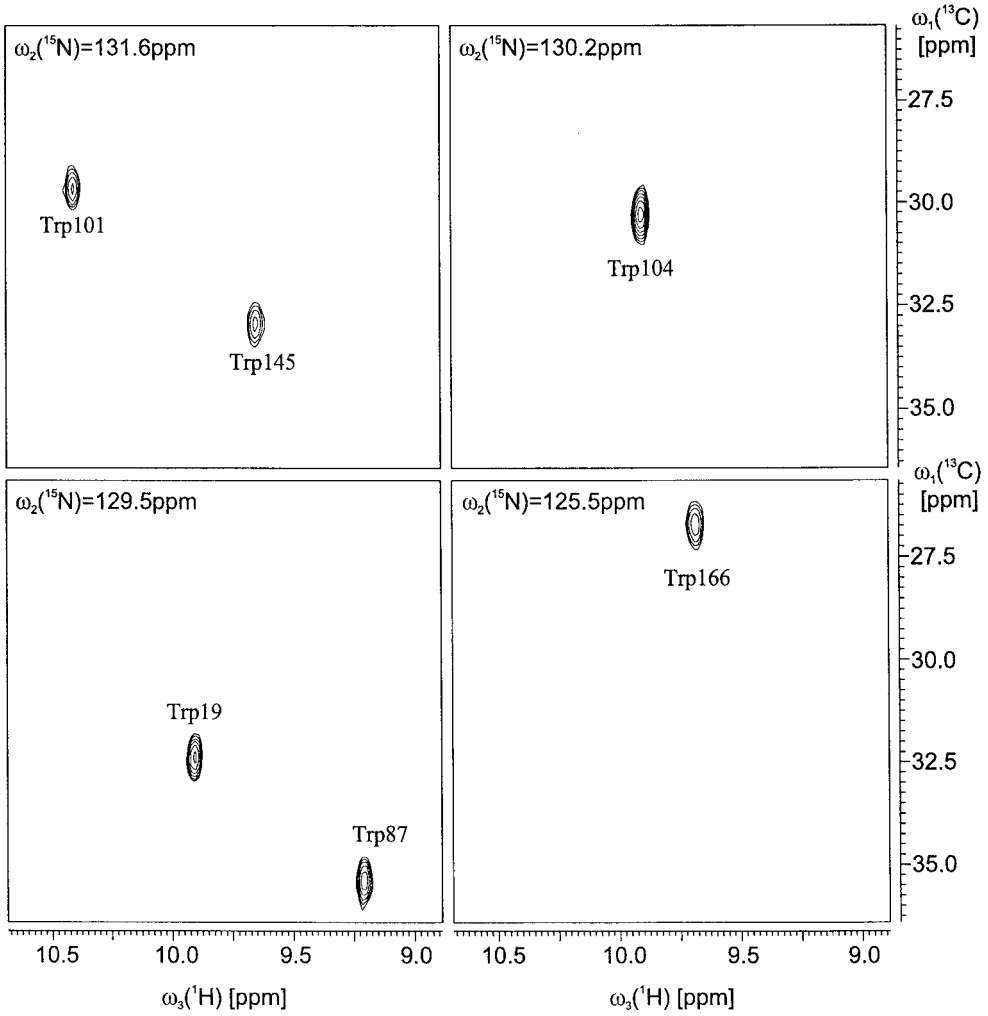

Figure 7. ω_1/ω_3 slices from a 3D [^{15}N, ^{1}H]-TROSY-HN(CDCG)CB spectrum (500 MHz) of ^{13}C/^{15}N-labelled xylanase, taken at the ^{15}N (ω_2) coordinates given in the upper left comers. A cross peak observed at $\omega_1(^{13}C) = 33.4$ ppm/$\omega_2(^{15}N) = 127.9$ ppm, which is assigned to Trp40, is not shown here.

cross peak observed in the corresponding ω_1/ω_3 slice at $\omega_2 = 120.3$ ppm (not shown). In contrast, the sixth residue, His181, did not give rise to a detectable cross peak, presumably because of a strong coupling effect between the $^{13}C^{\delta 2}$ and $^{13}C^{\gamma}$ spins which resonate within less than 1 ppm, thus preventing a proper magnetization transfer.

The set-up of the [^{15}N,^{1}H]-TROSY-HN(CDCG)CB experiment requires resonance positions of tryptophan ε2-, δ1- and γ-carbons be known exactly, because of the high selectivity of pulses on aromatic carbons in the sequence of Figure 2. For this purpose, two-dimensional experiments were initially performed, providing correlations of $^1H^{N\varepsilon 1}$ with the two adjacent carbons or with $^{13}C^{\gamma}$. The resulting [^{15}N, ^{1}H]-TROSY-H(N)C^{ar} spectra of xylanase and DFPase are shown in Figures 5A and 5B, respectively. Located in the region between 138 and 141 ppm along the ω_1 axis are $^{13}C^{\varepsilon 2}$ resonances, appearing as triplets due to two $^1J_{CC}$ interactions of approximately equal magnitude, while $^{13}C^{\delta 1}$ resonances, only split by one $^1J_{CC}$ coupling, are found in the 123–130 ppm region.

Depending on their solvent exchange characteristics, cross peaks involving nitrogen-bound protons in histidine side-chains can be detected, too. In these cases, correlations with imidazole $^{13}C^{\varepsilon 1}$ nuclei are identified by their lowfield chemical shift and the lack of multiplet fine structure. Both His162 of xylanase

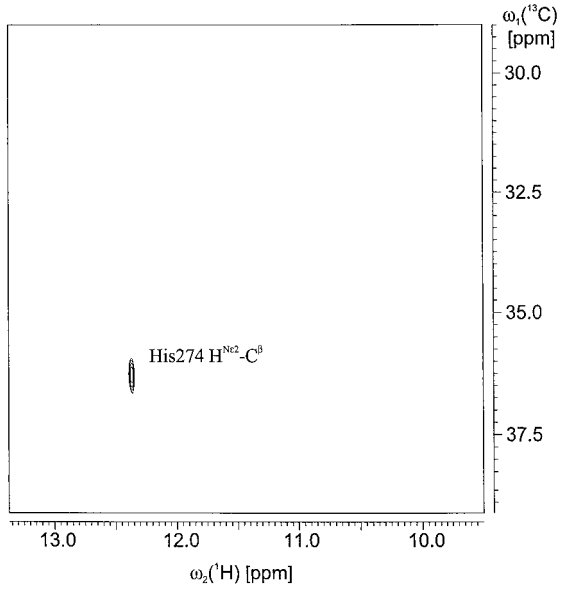

Figure 8. 2D [^{15}N, ^{1}H]-TROSY-HN(CDCG)CB spectrum of DFPase recorded at 600 MHz with a pulse sequence composed of elements from those of Figures 1 and 2 (see text for details) to selectively observe correlations for histidine side-chains. Note that the $^{13}C^{\beta}$ resonance of His274 is upfield shifted by 0.7 ppm from the position in the spectrum of Figure 4 because of the ^{2}H isotope shift in the perdeuterated compared to the fully protonated sample.

and His274 of DFPase are uncharged at the respective pH value of the samples and appear to be in the $N^{\varepsilon 2}$-H tautomeric state. Consequently, a second cross peak at the $^{13}C^{\delta 2}$ resonance position, typically in the range between 115 and 120 ppm, is observed, which exhibits a splitting due to the $^{1}J_{C\delta 2C\gamma}$ coupling. In contrast, His181 of DFPase, also unprotonated at pH = 6.5, is in the less abundant $N^{\delta 1}$-H tautomeric state, giving rise to a $^{1}H^{N\delta 1}$- $^{13}C^{\gamma}$ correlation at $\omega_1 = 127.8$ ppm. The latter is a heavily distorted doublet along the carbon dimension because of the strong coupling with the $^{13}C^{\delta 2}$ spin, which itself yields an additional weak cross peak at $\omega_1 = 127.1$ ppm, possibly through a two-bond scalar interaction with $^{15}N^{\delta 1}$. Shown in Figure 5C is a 2D [^{15}N, ^{1}H]-TROSY-H(NCD)CG spectrum of DFPase, providing $^{1}H^{N\varepsilon 1}$-$^{13}C^{\gamma}$ correlations in tryptophan side-chains. The partially resolved doublet-of-doublet structure along ω_1 reveals the presence of two $^{1}J_{CC}$ splittings of different sizes. The relayed $^{1}H^{N\varepsilon 2}$-$^{13}C^{\gamma}$ cross peak of His274 is aliased in the ω_1 dimension and corresponds to a $^{13}C^{\gamma}$ chemical shift of 139.4 ppm. In addition, a weak $^{1}H^{N\delta 1}$-$^{13}C^{\delta 2}$ cross peak for His181 was detected at $\omega_1 = 127.1$ ppm, which is outside the plotted region.

Knowledge of the relevant indole ^{13}C chemical shifts allows the fine-tuning of carbon pulse offsets to optimize the sensitivity of the [^{15}N, ^{1}H]-TROSY-HN(CDCG)CB sequence. Its application to DFPase in a two-dimensional version is illustrated in Figure 6. Each cross peak provides a $^{1}H^{N\varepsilon 1}$-$^{13}C^{\beta}$ connectivity, such that the indole resonances from five out of the six tryptophan residues could be unambiguously assigned because sequence specific $^{13}C^{\beta}$ chemical shifts were available from the standard backbone assignment protocol. In the perdeuterated DFPase sample, the Trp131 side-chain NH, missing in the spectra of Figures 5 and 6, does not give rise to a detectable signal in simple [^{15}N, ^{1}H]-TROSY or -HSQC experiments because of very slow back exchange upon transferring the protein into H_2O solution. However, a $^{1}H^{N\varepsilon 1}$-$^{13}C^{\beta}$ correlation was observed in a [^{15}N, ^{1}H]-TROSY-HN(CDCG)CB spectrum of a partially deuterated sample (results not shown), which had been prepared in a H_2O-based medium (Markus et al., 1994; Serber et al., 2001), where all indole NH protons are retained. In the case of xylanase $^{1}H^{N\varepsilon 1}$-$^{13}C^{\beta}$ connectivities were obtained for each of its seven tryptophan side-chains. Since two $^{1}H^{N\varepsilon 1}$ resonances overlap completely, the [^{15}N, ^{1}H]-TROSY-HN(CDCG)CB experiment was recorded in a three-dimensional fashion. As demonstrated in Figure 7, well separated cross peaks were obtained for Trp19 and Trp104 owing to the dispersion of $^{15}N^{\varepsilon 1}$ chemical shifts.

Despite the similar side-chain spin topology no [^{15}N, ^{1}H]-TROSY-HN(CDCG)CB signals were detected for those histidine residues seen in the spectra of Figure 5. This is due to the selective 180° pulse on tryptophan γ-carbons in the pulse sequence of Figure 2. While this may help to avoid confusion during the assignment of tryptophan resonances, observation of the corresponding histidine $^{1}H^{N\varepsilon 2}$-$^{13}C^{\beta}$ or $^{1}H^{N\delta 1}$-$^{13}C^{\beta}$ connectivities can be useful, especially when only a perdeuterated sample is available, precluding the application of the [^{13}C, ^{1}H]-TROSY-HCD(CG)CB sequence. As described in the Materials and methods section, the pulse sequences of Figures 1 and 2 can be combined to induce the magnetization transfer from slowly exchanging imidazole NH protons and histidine β-carbons. An experimental verification is given in Figure 8 which shows the $^{1}H^{N\varepsilon 2}$-$^{13}C^{\beta}$ cross peak of His274 in DFPase. To observe a similar correlation for histidines in the $N^{\delta 1}$-H tautomeric state the $C^{\delta}C^{\gamma}$-Relay step has to be omitted from the pulse sequence. However, an attempt to detect a $^{1}H^{N\delta 1}$-$^{13}C^{\beta}$ cross peak of His181 failed, again because of the strong coupling

between the two adjacent aromatic carbon spins in this particular residue.

If of interest, the ^{15}N chemical shifts of slowly exchanging imidazole NH groups can be sampled simply by recording the [^{15}N, ^{1}H]-TROSY-HNC^{ar} in a three-dimensional manner, although they are, of course, available from a regular [^{15}N, ^{1}H]-TROSY as well. To assign the unprotonated nitrogen resonances or those of protonated, fast exchanging nitrogens, they might be correlated to the $^{1}H^{\delta 2}/^{13}C^{\delta 2}$ chemical shifts known from the [^{13}C, ^{1}H]-TROSY-HCD(CG)CB experiment using methods such as HCN (Sudmeier et al., 1996), which can also be implemented as a [^{13}C, ^{1}H]-TROSY version (Fiala et al., 2000; Riek et al., 2001).

Conclusions

Efficient TROSY-based pulse sequences have been presented to link aromatic proton and carbon or nitrogen resonances of histidine and tryptophan side-chains with the respective β-carbon chemical shifts. In combination with established backbone NH-based triple-resonance experiments sequence-specific aromatic resonance assignment can thus be obtained without relying on NOE information, which is often ambiguous. Both methods are applicable to ^{13}C/^{15}N-labelled, medium-sized proteins, whereas for larger proteins the tryptophan side-chain assignment experiment requires additional deuteration. With its ability to extend sequence-specific assignments to aromatic ring systems in perdeuterated proteins, too, this experiment contrasts with methods previously proposed for the same purpose.

Acknowledgements

Financial support from the Fraunhofer-Gesellschaft (grant E/B31E/MO157/M5137) is gratefully acknowledged. The recombinant enzyme xylanase was produced in collaboration with Novo-Nordisk A/S (Bagsvaerd, Denmark). All measurements were carried out at the Large Scale Facility for Biomolecular NMR at the University of Frankfurt (Germany).

References

Andersson, P., Annila, A. and Otting, G. (1998) *J. Magn. Reson.*, **133**, 364–367.

Bax, A. and Freeman, R. (1981) *J. Magn. Reson.*, **44**, 542–561.

Bax, A., Clore, G.M. and Gronenborn. A.M. (1990) *J. Magn. Reson.*, **88**, 425–431.

Bax, A., Griffey, R.H. and Hawkins, B.L. (1983) *J. Magn. Reson.*, **55**, 301–315.

Bendall, M.R., Pegg, D.T. and Doddrell, D.M. (1983) *J. Magn. Reson.*, **52**, 81–117.

Billeter, M., Braun, W. and Wüthrich, K. (1982) *Mol. Biol.*, **155**, 321–346.

Boyd, J. and Soffe, N. (1989) *J. Magn. Reson.*, **85**, 406–413.

Brutscher, B., Boisbouvier, J., Pardi, A., Marion, D. and Simorre, J.-P. (1998) *J. Am. Chem. Soc.*, **120**, 11845–11851.

Carlomagno, T., Maurer, M., Sattler, M., Schwendinger, M.G.. Glaser, S.J. and Griesinger, C. (1996) *J. Biomol. NMR*, **8**, 161–170.

Czisch, M. and Boelens, R. (1998) *J. Magn. Reson.*, **134**, 158–160.

Dingley, A.J. and Grzesiek, S. (1998) *J. Am. Chem. Soc.*, **120**, 8293–8297.

Eletsky, A., Kienhofer, A. and Pervushin, K. (2001) *J. Biomol. NMR*, **20**, 177–180.

Emsley, L. and Bodenhausen, G. (1990) *Chem. Phys. Lett.*, **165**, 469–476.

Fesik. S.W., Eaton, H.L., Olejniczak, E.T., Zuiderweg, E.R.P., McIntosh, L.P. and Dahlquist, F.W. (1990) *J. Am. Chem. Soc.*, **112**, 886–888.

Fiala, R., Czernek, J. and Sklenář, V. (2000) *J. Biomol. NMR*, **16**, 291–302.

Grzesiek. S. and Bax. A. (1992) *J. Am. Chem. Soc.*, **114**, 6291–6293.

Grzesiek, S. and Bax, A. (1993) *J. Am. Chem. Soc.*, **115**, 12593–12594.

Grzesiek, S. and Bax, A. (1995) *J. Am. Chem. Soc.*, **117**, 6527–6531.

Grzesiek, *S.*, Anglister. J., Ren, H. and Bax, A. (1993) *J. Am. Chem. Soc.*, **115**, 4369–4370.

Hartleib. J. and Rüterjans, H. (2001) *Protein Expr. Purif.*, **21**, 210–219.

Ikura, M., Kay, L.E. and Bax, A. (1990) *Biochemistry*, **29**, 4659–4667.

Kay, L.E., Ikura, M. and Bax, A. (1990) *J. Am. Chem. Soc.*, **112**, 888–889.

Löhr, F. and Rüterjans, H. (1996) *J. Magn. Reson.*, **B112**, 259–268.

Löhr, F., Pfeiffer, S., Lin, Y.-J., Hartleib, J., Klimrnek, O. and Rüterjans, H. (2000) *J. Biomol. NMR*, **18**, 337–346.

Loria, J.P., Rance, M. and Palmer III, A.G. (1999) *J. Magn. Reson.*, **141**, 180–184.

Marion, D., Ikura, M., Tschudin, R. and Bax, A. (1989) *J. Magn. Reson.*, **85**, 393–399.

Markus, M.A., Dayie, K.T., Matsudaira, P. and Wagner, G. (1994) *J. Magn. Reson.*, **B105**, 192–195.

Matsuo, H., Kupče, Ė., Li, H. and Wagner, G. (1996) *J. Magn. Reson.*, **B111**, 194–198.

Meissner, A. and Sørensen, O.W. (1999) *J. Magn. Reson.*, **139**, 439–442.

Morris, G.A. and Freeman, R. (1979) *J. Am. Chem. Soc.*, **101**, 760–762.

Patt, S. (1992) *J. Magn. Reson.*, **96**, 94–102.

Pervushin, K., Riek, R., Wider, G. and Wüthrich, K. (1997) *Proc. Natl. Acad. Sci. USA*, **94**, 12366–12371.

Pervushin, K., Riek, R., Wider, G. and Wüthrich, K. (1998a) *J. Am. Chem. Soc.*, **120**, 6394–6400.

Pervushin, K., Wider, G. and Wüthrich, K. (1998b) *J. Biomol. NMR*, **12**, 345–348.

Prompers, J.J., Groenewegen, A., Hilbers, C. W. and Pepermans, H.A.M. (1998) *J. Magn. Reson.*, **130**, 68–75.

Rance, M., Loria, J.P. and Palmer III, A.G. (1999) *J. Magn. Reson.*, **136**, 92–101.
Riek, R., Pervushin, K., Fernández, C., Kainosho, M. and Wüthrich, K. (2001) *J. Am. Chem. Soc.*, **123**, 658–664.
Sabini, E., Sulzenbacher, G., Dauter, M., Dauter, Z., Jorgensen, P.L., Schulein, M., Dupont, C., Davies, G.J. and Wilson, K.S. (1999) *Chem. Biol.*, **6**, 483–492.
Salzmann, M., Pervushin, K., Wider, G., Senn, H. and Wüthrich, K. (1998) *Proc. Natl. Acad. Sci. USA*, **95**, 13585–13590.
Salzmann, M., Wider, G., Pervushin, K. and Wüthrich, K. (1999a) *J. Biomol. NMR*, **15**, 181–184.
Salzmann, M., Wider, G., Pervushin, K., Senn, H. and Wüthrich, K. (1999b) *J. Am. Chem. Soc.*, **121**, 844–848.
Serber, Z., Ledwidge, R., Miller, S.M. and Dötsch, V. (2001) *J. Am. Chem. Soc.*, **123**, 8895–8901.
Shaka, A.J., Barker, P.B. and Freeman, R. (1985) *J. Magn. Reson.*, **64**, 547–552.
Shaka, A.J., Keeler, J., Frenkiel, T. and Freeman, R. (1983) *J. Magn. Reson.*, **52**, 335–338.
Stonehouse, J., Shaw, G.L., Keeler, J. and Laue, E.D. (1994) *J. Magn. Reson.*, **A107**, 178–184.
Sudmeier, J.L., Ash, E.L., Günther, V.L., Luo, X., Bullock, P. A. and Bachovchin, W. W. (1996) *J. Magn. Reson.*, **B113**, 236–247.
Venters, R.A., Metzler, W.J., Spicer, L.D., Mueller, L. and Farmer II, B.T. (1995) *J. Am. Chem. Soc.*, **117**, 9592–9593.
Wagner, G. and Wüthrich, K. (1982) *J. Mol. Biol.*, **155**, 347–366.
Weigelt, J. (1998) *J. Am. Chem. Soc.*, **120**, 10778–10779.
Wittekind, M. and Mueller, L. (1993) *J. Magn. Reson.*, **B101**, 201–205.
Wüthrich, K. (1986) *NMR of Proteins and Nucleic Acids*, Wiley, New York, NY.
Yamazaki, T., Forman-Kay, J.D. and Kay, L.E. (1993) *J. Am. Chem. Soc.*, **115**, 11054–11055.
Yan, X., Kong, X., Xi a, Y., Sze, K.H. and Zhu, G. (2000) *J. Magn. Reson.*, **147**, 357–360.
Yang, D. and Kay, L.E. (1999) *J. Biomol. NMR*, **14**, 273–276.
Zhu, G., Kong, X.M., Yan, X.Z. and Sze, K.H. (1998) *Angew. Chem. Int. Ed. Engl.*, **37**, 2859–2861.